Journal of Alloys and Compounds 509 (2011) 704–711

Contents lists available at ScienceDirect

Journal of Alloys and Compounds

journal homepage: www.elsevier.com/locate/jallcom

Microstructure and mechanical properties of Mg–Al–Mn–Ca alloy sheet produced by twin roll casting and sequential warm rolling

Yinong Wang[a,b], Suk Bong Kang[b,*], Jaehyung Cho[b]

[a] School of Materials Science and Engineering, Dalian University of Technology, Dalian 116026, PR China
[b] Korea Institute of Materials Science, Changwon 641-010, Republic of Korea

ARTICLE INFO

Article history:
Received 6 August 2009
Received in revised form 29 July 2010
Accepted 29 July 2010
Available online 5 August 2010

Keywords:
Magnesium alloys
Twin roll casting
Microstructure
Mechanical properties

ABSTRACT

Microstructural evolution and mechanical properties of twin roll cast (TRC) Mg–3.3 wt.%Al–0.8 wt.%Mn–0.2 wt.%Ca (AM31 + 0.2Ca) alloy strip during warm rolling and subsequent annealing were investigated in this paper. The as-TRC alloy strip shows columnar dendrites in surface and equiaxed dendrites in center regions, as well as finely dispersed primary Al_8Mn_5 particles on interdendritic boundaries which result in the beneficial effect on microstructural refinement of strip casting. The warm rolled sheets show intensively deformed band or shear band structures, as well as finely and homogeneously dispersed Al–Mn particles. No evident dynamic recrystallization (DRX) takes place during warm rolling process, which is more likely attributed to the finely dispersed particle and high solid solution of Al and Mn atoms in α-Mg matrix. After annealing at 350 °C for 1 h, the warm rolled TRC sheets show fine equiaxed grains around 7.8 μm in average size. It has been shown that the present TRC alloy sheet has superior tensile strength and comparative elongation compared to commercial ingot cast (IC) one, suggesting the possibility of the development of wrought magnesium alloy sheets by twin roll strip casting processing. The microstructural evolution during warm rolling and subsequent annealing as well as the resulting tensile properties were analyzed and discussed.

1. Introduction

Magnesium alloys have a great potential for application in lightweight structural parts owing to their low density, excellent specific strength and stiffness, as well as good castability and machinability. In the past decade, the application of magnesium alloys for lightweight structural components has significantly increased due to a rapid expansion of high pressure die-casting components in the automobiles by using near net-shape die-casting technology [1,2]. Because the wrought magnesium alloy is usually expensive and is poor in formability at room temperature compared to the conventional cast one, there is still a lack of competitive magnesium wrought products, especially sheet materials, which are necessary for various weight-saving applications, although the wrought magnesium alloys are known to offer generally better mechanical properties than that of ingot cast (IC) magnesium alloys [3–5]. So, the reduction of manufacturing costs and the improvement of formability are significantly required.

Recently, twin roll casting (TRC) is paid a great attention on economically fabricating wrought magnesium alloy sheets from the melt [6–12], which combines continuous strip casting and direct hot rolling into a single step, having an advantage of one-step processing for flat rolled products. Besides being such a cost-effective process, TRC process also has benefit effects on resulting microstructure such as reducing segregation, improving inclusion size distribution and refining microstructural homogeneity. In this respect, it is mostly believed that the TRC process can be an alternative for the production of magnesium alloy sheets.

For improving the strength and the formability of the wrought magnesium alloys, it seemed to be effective to obtain uniform fine microstructure (grain and particle) and well-distributed texture in-plane. It is well known the high solidification rate has enable the utilization of dispersion strengthening and solid solution strengthening by alloying elements which have limited solubilities in Mg matrix, which are usually avoided in ingot casting because these elements form coarse intermetallic particles at low solidification rate. So, it is expected that such dispersion strengthening and solid solution strengthening can be utilized in twin roll strip casting with a relatively high solidification rate ranging from 10^2 K/s to 10^3 K/s [13], which is a semi-rapid solidification processing.

The present research is aimed at studying the feasibility of TRC strip for the production of magnesium alloy sheets. The microstructural evolution of twin roll strip cast alloy subjected to multiple-pass warm rolling and subsequent annealing has been investigated, and the resulting tensile properties were analyzed on

* Corresponding author. Tel.: +82 55 280 3301; fax: +82 55 280 3599.
E-mail address: sbkang@kims.re.kr (S.B. Kang).

0925-8388/$ – see front matter © 2010 Elsevier B.V. All rights reserved.
doi:10.1016/j.jallcom.2010.07.183

Table 1
Chemical composition of the present AM31 + 0.2Ca alloys (mass content, %).

Alloy	Al	Mn	Ca	Mg
TRC	3.27	0.52	0.12	Bal.
IC	3.37	0.59	0.14	Bal.

fine particle dispersion strengthening, solid solution strengthening and fine-grain strengthening as compared to those of conventional IC alloy. The present alloy investigated is AM31 + 0.2Ca (Mg–3.3 wt.%Al–0.8 wt.%Mn–0.2 wt.%Ca in nominal composition), where Al is added for giving rise to solid solution strengthening, Mn for inducing the dispersion of Al–Mn compound, and Ca for preventing ignition and oxidation during melting. Furthermore, the addition of Ca can evidently refine grains, and improve elevated temperature properties and corrosion resistance of magnesium alloys [14–16].

2. Experimental procedures

A horizontal type twin roll caster with water cooling system was used to fabricate AM31 + 0.2Ca magnesium alloy strip. A pair of copper alloy rollers with 300 mm in diameter was used for the horizontal type twin roll caster. Pure magnesium and aluminum ingots were used to produce AM31 + 0.2Ca alloy. Mn and Ca elements were added in the form of Al–10 wt.%Mn and Mg–30 wt.%Ca master alloys, and SF_6 and CO_2 shield gas were used to protect the molten alloy. The alloying elements of Al, Al–Mn and Mg–Ca master alloys were added to the molten magnesium at 750 °C, and the melt was held at 750 °C for 30 min to ensure that the alloying elements were completely dissolved and diffused. For the ingot cast (IC) processing, the molten alloy was poured at 720 °C into a steel mold with a size of 180 mm × 160 mm × 25 mm. The chemical composition of the experimental alloys was analyzed and shown in Table 1. For TRC processing, the molten alloy was flowed down the cooling slope into the casting tundish, and then molten alloy in the tundish is dragged onto the surface of the rotating rollers. The molten alloy solidifies very soon after leaving the casting tundish due to the contact with cooled roller and is rolled between the upper and lower rollers. The rolling speed was 3–3.25 rpm and the roller gap was 3 mm. A twin roll casting strip with 4.0 mm thick, 180 mm wide and 10 m long was manufactured. The chemical composition of the TRC alloy was analyzed and shown in Table 1.

Warm rolling and subsequent annealing were performed to obtain the wrought magnesium alloy sheet with equiaxed and fine-grained microstructure. Before warm rolling, the twin roll casting strip were reheated to 350 °C for 30 min and then rolled on a two-roller mill with a roller diameter of 200 mm. The rollers were preheated to 250 °C and operated at a speed of 3.5 rpm. The samples were reheated to 350 °C for 5 min between each pass. Warm rolling was carried out up to a total reduction of ~86% achieved over seven passes to reduce the strip thickness from 4.0 mm to 0.56 mm, and final annealing at 350 °C for 60 min was applied. For comparable study, a slab with 4 mm thick was cut out of cast ingot, and warm rolling and annealing were performed on the same schedule with the twin roll casting strip described above as a reference alloy.

All samples for optical microscopy (OM) were sectioned, cold-mounted, polished and then etched in a solution of picric acid (5 g), acetic acid (10 ml), distilled water (10 ml) and ethanol (100 ml). The average grain size and average particle size were analyzed from several micrographs from longitudinal sections using a computer-aided liner intercept measurement. Scanning electron microscopy (SEM) and energy dispersive spectroscopy (EDS) were used to study the morphology and micro-chemical characterization of second phases. All phases were estimated and deduced according to the combination of phase diagrams and atomic ratio of elements which possibly form stable or metastable phases. Precipitates and deformed substructures were examined by using JEM-2100F transmission electron microscopy (TEM) operating at 200 kV. Thin foil were prepared by twin-jet polishing using a solution of $HClO_4$ (5%), butanol (35%) and methanol (65%), and then by ion beam milling with an incident angle of 3° for 30 min.

Tensile test was conducted using an Instron 4206 universal testing machine equipped with 10 mm gauge extensometer. The rolled sheets were machined into ASTM E8 tensile samples with a 3 mm gauge width and 12 mm gauge length. All tensile tests were carried out with an initial strain rate of $1 \times 10^{-3}\ s^{-1}$ at ambient temperature, where the tensile direction was the same as the rolling direction.

3. Results

3.1. Microstructure of twin roll cast strip

Fig. 1 shows the optical microstructure of the longitudinal section of TRC AM31 + 0.2Ca alloy strip. It can be seen that the microstructure of TRC strip was different from the surface to the center. The columnar dendrites are observed in surface and oriented 45–80° along the cast rolling direction, which are mainly the result of coupling between the directional solidification and subsequent hot deformation during TRC process, as shown in Fig. 1a. The columnar to equiaxed transition occurs in mid-thickness region, as shown in Fig. 1b. Distinct macro-segregation through the thickness of TRC strip was not found. The similar microstructure of the present AM31 + 0.2Ca strip was also reported on AZ21 and AZ31 TRC strips [17,18].

The difference of microstructures between the surface and the center of the strip is attributed to the different solidification rate through the thickness of the strip during the horizontal twin roll strip casting. The molten metal directly contacted with the copper roller cooled with water inside, which results in the higher cooling rate in the surface region than that in the center region. The dendrite structure was developed from the surface to center of the strip along the thermal gradient. Secondary dendrite arm spacing (SDAS) was measured to approximately estimate the cooling rate during the strip casting. It is shown that the SDAS of the strip varies from ~3.4 μm in the surface region to ~5.6 μm in the center region. As expected, the center of the strip shows the largest SDAS, suggesting that it experiences the lowest cooling rate. The cooling rate was estimated from the measured SDAS by the following relationship [17]:

$$\mathrm{SDAS} = 5.3 t_f^{0.43}, \quad R = \frac{\Delta T_f}{t_f}$$

where t_f is local solidification time (s), R is cooling rate (K/s) and ΔT_f is non-equilibrium temperature range of solidification, which is approximately 75 K for the present AM31 + 0.2Ca alloy. The cooling rate undergone during the AM31 + 0.2Ca strip casting ranges approximately from 80 K/s to 200 K/s, which are higher than those undergone during conventional ingot casting process (~10 K/s).

A closer observation on the microstructures of as-TRC strip reveals the existence of smaller primary dispersed particles located on the interdendritic boundaries, as shown in Fig. 2. The average size of these dispersed particles is around ~1 μm. Fig. 3 shows the SEM micrograph of ingot cast one, where the large polygonal and relatively small round particles as well as some acicular phases are presented either along the grain boundaries or inside the grains. From Figs. 2 and 3, it can be clearly seen that the size of these particles of as-TRC strip is much smaller than that of as-IC sample.

Energy dispersive spectroscopy (EDS) analysis indicated that most of primary dispersed particles mainly comprised of Al and Mn elements with 1.08–1.98 of Al/Mn atomic ratio in both TRC strip and ingot cast alloy. Based on the atomic ratios of Al–Mn from Al–Mn binary phase diagrams [19], it could be deduced that these dispersed particles are mainly identified as Al_8Mn_5 phases, which are consistent with the previous studies [20,21]. Moreover, the acicular phases presented in the as-ingot alloy are mainly identified as $(AlMg)_2Ca$ phase, which was studied in detail by Han [22]. Also, the EDS results showed that the average compositions of Al and Mn elements in the α-Mg matrix of as-TRC strip are about ~2.25 wt.% and ~0.46 wt.%, respectively, which are much higher than that of as-IC sample, where the average compositions of Al and Mn atoms in the α-Mg matrix are about ~1.88 wt.% and ~0.24 wt.%, respectively. It could be concluded that the differences in size of the primary precipitate particles and in solid solubility of Al and Mn in α-Mg matrix between as-TRC and as-IC samples are also attributed to the different solidification rate during the process. As expected, as-TRC strip shows the higher solidification rate than that of as-IC sample, which results in the more fine primary dispersed particles and higher solid solubility of Al and Mn atoms in the α-Mg matrix.

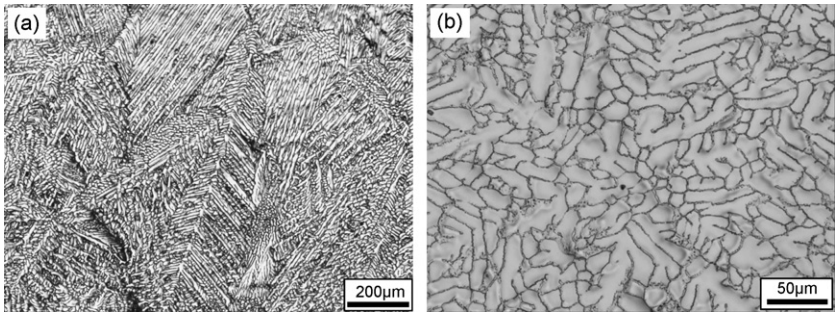

Fig. 1. Optical micrographs of as-TRC strip in roll side (a) and center (b). Rolling direction is parallel to the scale bar.

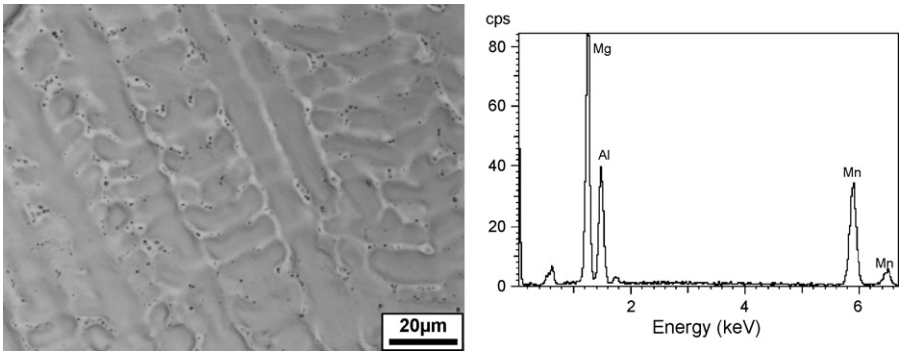

Fig. 2. Typical OM morphology (left) and EDS (right) of primary Al_8Mn_5 particles in as-TRC strip.

3.2. Microstructure of warm rolled sheets

Fig. 4 shows the optical microstructure of TRC AM31 + 0.2Ca strip warm rolled at 350 °C with different rolling reduction ratios. After the first pass of 30% thickness reduction (Fig. 4a), deformed dendrite structure can be clearly seen. A large amount of dendrite arms and dendrite cells were elongated and had a trend to parallel to the rolling direction. No evident twins were found. On further reduction to 67% (Fig. 4b), more and more deformation bands or shear bands extensively developed, and spacing between deformation bands or shear bands became more narrow. When thickness reduction reached 80% (Fig. 4c), especially 86% (Fig. 4d), a homogeneous deformation microstructure was obtained. Moreover, a remarkable dynamically recrystallizied (DRXed) microstructure was not observed. From the optical microstructural evolution during the whole warm rolling process, as shown in Fig. 4, it can be seen that deformed dendrite and deformation bands or shear bands were gradually developed, and no evident twins and DRXed grains were observed. These findings indicated that most of the rolling strain is mainly accommodated by dislocation multiplication mechanism.

Fig. 5 shows the optical microstructures of IC AM31 + 0.2Ca sample warm rolled at 350 °C with different rolling reduction ratios. After the first pass of 30% thickness reduction, twinning occurs extensively at the initial stage of the warm rolling in IC sample, indicating that most of the rolling strain is mainly accommodated by twinning, as shown in Fig. 5a. Most of the twins are considered to be $\{1\,0\,-1\,2\}$ twinning which is most easily activated in Mg [23]. Concurrently, small DRXed grains can be observed at the twinned regions. On further reduction to 67% (Fig. 5b), more and more DRXed grains are continuously nucleated in the twinned regions. It is often observed that the size of DRXed grains can be estimated by the width of twins, suggesting that the nucleation of DRXed grains is closely related to the specific mechanism associated with the twinning [24]. When the thickness reduction is 80% (Fig. 5c), small DRXed grains developed at grain boundaries, forming typical necklace structures and the entire microstructure becomes significantly inhomogeneous. It is clear that some of the grains are sensitive to DRX, and thus are quickly replaced by fine DRXed grains. On the other hand, some of the grains are insensitive to DRX, which are still present with a large grain size in the microstructure. The

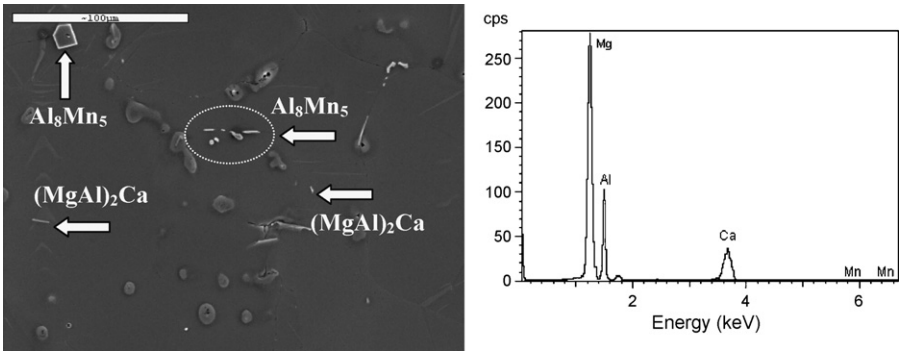

Fig. 3. SEM morphology of Al_8Mn_5 and $(MgAl)_2Ca$ particles (left) and EDS of $(MgAl)_2Ca$ particle (right) of in as-IC sample.

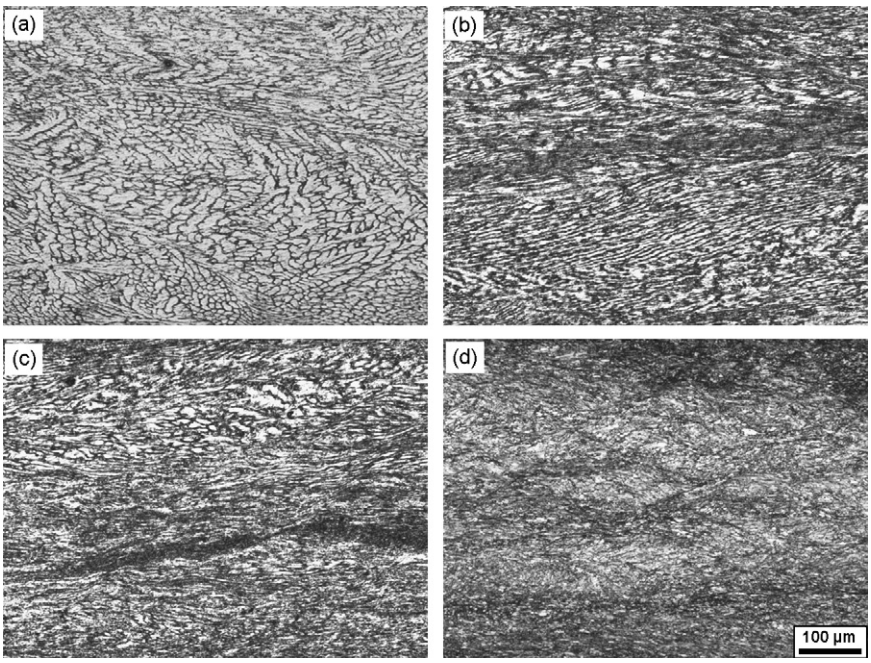

Fig. 4. Typical microstructure of TRC sample rolled at 350 °C with different rolling reduction: (a) 30% (1-pass), (b) 67% (3-pass), (c) 80% (5-pass) and (d) 86% (7-pass). Longitudinal sections with RD parallel to scale bar.

inhomogeneous microstructure is mainly attributed to the uneven rate of recrystallization among different oriented grains. Moreover, the shear band-like fine grains are clearly observed, which may easily accommodate the strain imposed by warm rolling. Obviously, these shear band-like fine grains would probably have a close relationship to the DRXed grains nucleated in the twinned regions. With a reduction increase from 80% (5-pass) to 86% (7-pass), some relatively large grains were refined by DRX processing, resulting in a relatively homogenous microstructure, as shown in Fig. 5d. It can be seen that the microstructural evolution of TRC and IC samples during the whole warm rolling process has a significant difference from each other.

Moreover, the polished sample without etching reveals the microstructures of particle distribution. Fig. 6a and b shows the microstructures of particle distribution in TRC and IC samples subjected to the final warm rolling (86% reduction), respectively. Finely and homogeneously distributed particles with average diameter of ~0.8 μm were clearly observed throughout the sample of TRC sheet, as show in Fig. 6a. However, inhomogeneously dispersed large particles with ~6.5 μm in average diameter are obviously observed in

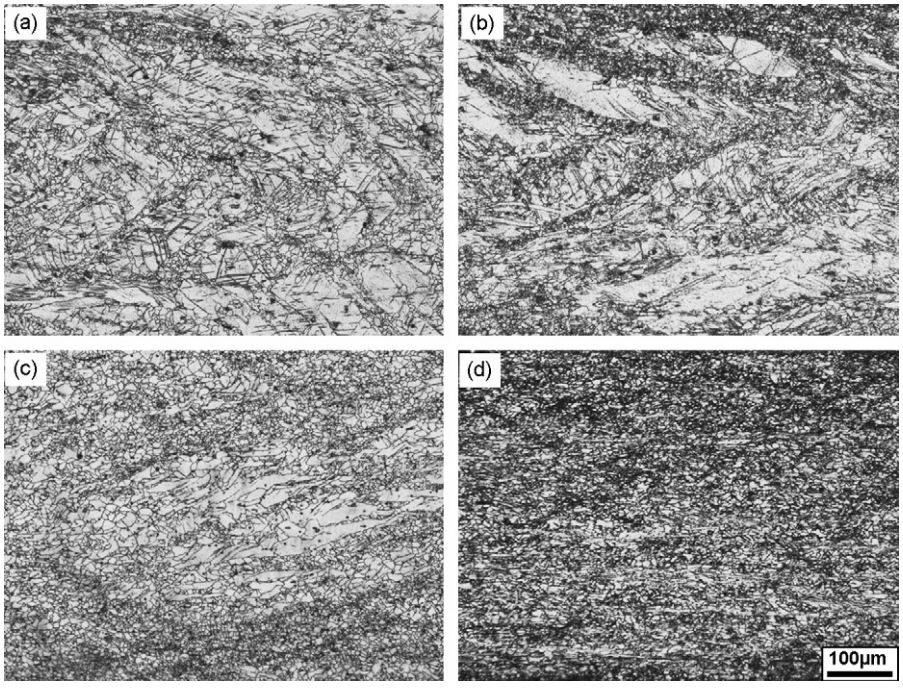

Fig. 5. Typical microstructure of IC samples rolled at 350 °C with different rolling reduction: (a) 30% (1-pass), (b) 67% (3-pass), (c) 80% (5-pass) and (d) 86% (7-pass). Longitudinal sections with RD parallel to scale bar.

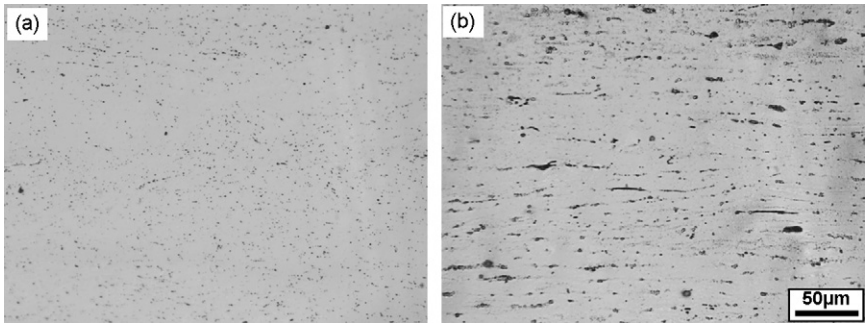

Fig. 6. Optical micrographs of particles distributed in finial warm rolled (86% reductions) TRC (a) and IC (b) samples. Longitudinal sections with RD parallel to scale bar.

IC alloy, as seen in Fig. 6b, and some relatively small particles with 1–3 μm in diameter tend to arrange in lines, indicating that they are fragmented from original large particles during warm rolling process. Therefore, it is believed that the more fine and homogeneously distributed particles in the final warm rolled TRC sheet (Fig. 6a) is attributed to the original fine and uniform dispersed particles of as-TRC strip (Fig. 2a).

From these experimental results mentioned above, it can be seen that the warm rolling deformation behavior is remarkably different between TRC and IC samples. The predominant deformation behavior of TRC sample is mainly controlled by dislocation slip mechanism during the warm rolling. However, the predominant deformation behavior of IC sample during the warm rolling is mainly dominated by dynamic recrystallization (DRX). So, it is believed that the differences in the predominant deformation behavior must be attributed to the different as-received microstructures of TRC and IC samples.

3.3. Microstructure of annealed sheets

After the same final-step warm rolling (86% reduction, 7-pass), TRC and IC samples were annealed at 350 °C for 60 min. The optical microstructures of grained structure are shown in Fig. 7. It can be seen from Fig. 7a that the annealing of warm rolled TRC sheet resulted in fine-grained and equiaxed microstructure, indicating that homogeneous nucleation and grain growth occurred during static recrystallization. The main grain size was measured to be around 7.8 μm. For the warm rolled IC sample, grain growth takes place during the annealing, as shown in Fig. 7b. The measured grain size is around 11.2 μm, which is larger than that of twin roll cast one. Moreover, some large particles with ~10 μm in diameter are obviously observed in Fig. 7b. However, owing to smaller size of particles and low magnification of microstructure, finely and homogeneously dispersed particles are invisible in TRC sample, as shown in Fig. 7a. Higher magnification of microstructure of TRC sheet reveals that although there is no visible tendency for particles to preferentially lie on grain boundaries, some of the fine particles located on grain boundaries would restrain the migration of grain boundaries, which is one of the main reasons for obtaining the homogeneous fine-grained microstructure.

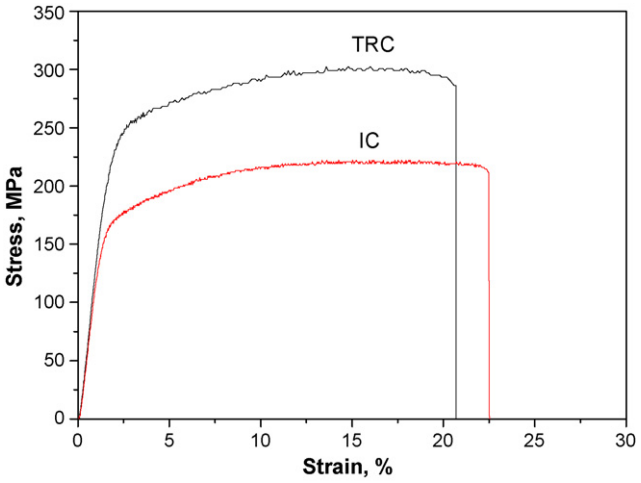

Fig. 8. Tensile stress–strain curves of post-annealed TRC and IC samples at room temperature.

Based on comparison of microstructures between TRC and IC samples after final warm rolling and subsequent annealing, it can lead that there are (1) more homogeneous fine-grained microstructure and (2) more homogeneously distributed fine particles which are expected to be resulted in superior mechanical properties. Microstructural parameters and mechanical properties of the present warm rolled and annealed TRC and ingot cast sheets are summarized in Table 2.

3.4. Mechanical properties of annealed sheets

Typical stress–strain curve from tensile tests in warm rolled and annealed TRC and IC AM31 + 0.2Ca samples is shown in Fig. 8. The

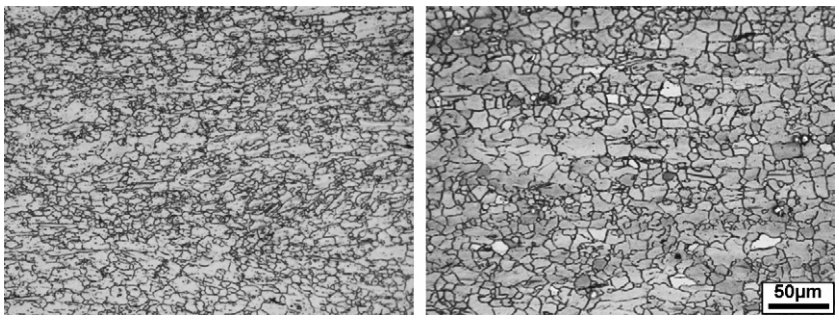

Fig. 7. Optical microstructures of grained structure and particle distribution in post-annealed TRC (a) and IC (b) samples. Longitudinal sections with RD parallel to scale bar.

Table 2
Microstructural parameters and mechanical properties of post-annealed TRC and IC samples.

Alloy	Ave. grain size (μm)	Ave. particle size (μm)	YS (MPa)	UTS (MPa)	Elongation (%)
TRC	~7.8	~0.8	~237	~300	~20.8
IC	~11.2	~6.5	~162	~220	~22.4

tensile properties are also summarized in Table 2. It can be seen that TRC sheet shows much higher yield stress (YS) (~237 MPa) and ultimate tensile stress (UTS) (~300 MPa) and comparative elongation (~20.8%) than those of ingot cast sheets, where YS, UTS and elongation are ~162 MPa, ~220 MPa, and ~22.4%, respectively. As expected, TRC sheet shows superior mechanical properties compared to ingot cast sheet after warm rolling and subsequent annealing, which is attributed to the microstructures of TRC sheet mentioned above.

4. Discussion

The microstructure of as-TRC strip is characterized by the high solid solubility of Al and Mn atoms and fine primary precipitate particles. For the Mg–Al based alloy system, Al is usually added into Mg matrix to give rise to solid solution strengthening and Mn is added to induce dispersion of Al–Mn intermetallic compounds to give rise to dispersion strengthening. Under the condition of conventional ingot casting, it is considered that the Mn has little solid solubility in α-Mg matrix based on the Mg–Mn binary phase diagram [25]. However, in the present study, Al, particularly Mn, have a large solid solubility in α-Mg matrix owing to rapid solidification during twin roll casting compared to conventional ingot casting. The difference of compositions in the α-Mg matrix seems to indicate that there is relatively much difference in the deformation mode of α-Mg matrix in two alloys.

In the present study, the microstructural evolution of conventional IC sample during warm rolling at medium temperature of 350 °C is mainly described as twining and twining induced DRX, as well as conventional DRX including continuous and discontinuous DRX [26], as shown in Fig. 5. However, for TRC sample, the microstructural evolution during warm rolling process is mainly characterized by deformation bands or shear bands, no evident twins and DRXed grains are observed, as shown in Fig. 4. Therefore, it is suggested that deformation mode for TRC sample is mainly dominated by dislocation multiplication mechanism. The warm rolled microstructures were examined using TEM, and typical example is shown in Fig. 9. In TRC sample after final warm rolling, well-defined subgrain boundaries with high density dislocations are clearly observed, indicating that dislocation multiplication slips, in particular, non-basal $\langle c+a\rangle$ slips on pyramidal slip system extensively occurred, as shown in Fig. 9a. However, in IC sample after final warm rolling, well-defined high angle grain boundaries can be observed, indicating that fully DRX took place, as shown in Fig. 9b. The results examined by TEM are in agreement with that by optical microscopy (OM).

Previous reports reveal that the $\{10\bar{1}2\}$ tensile twinning or $\{10\bar{1}1\}$–$\{10\bar{1}2\}$ double-twinning is most easily activated in Mg, and occur extensively at the early and later stage during compressive test or rolling at low and moderate temperature ranges for the Mg–Al–Zn (Mn) system alloys [23,26–28], which is similar to the present IC sample, as shown in Fig. 5a. However, no twins were found at the early and later stage during warm rolling in the present TRC sample, as shown in Fig. 4a. Therefore, it is mostly suggested that twinning and DRX are suppressed by high solid solubility of Mn in α-Mg matrix and fine dispersed particles in the present TRC strip.

In Mg, the $\{0002\}\langle 11\bar{2}0\rangle$ basal slip as well as $\{10\bar{1}2\}\langle 10\bar{1}1\rangle$ twinning usually take place preferentially because their critical resolved shear stresses (CRSS) are much lower than those for non-basal slip at room temperature. However, the basal slip has only two independent slip systems and the $\{10\bar{1}2\}$ twinning only provides the limited plastic strain (0.13). This gives rise to the poor ductility and formability of Mg and its alloys at room temperature, because five independent slip systems are necessary to make a polycrystalline materials undergo a general isotropic deformation without producing cracks. The CRSSs of various deformation systems of Mg at elevated temperatures are summarized by Chino and Mubuchi [29], as shown in Table 3. It is seen from Table 3 that the CRSS of non-basal slip decreases with an increase in temperature, and tension twinning is almost independent of temperature. At temperature of 350 °C imposed in the present experiment, the CRSSs of non-basal slips and tension twinning are almost the same, which would result in the combination of twin-DRX and continuous-DRX at the early stage of rolling in IC sample, as shown in Fig. 5. However, no evident twinning takes place in the TRC sample. Therefore, it is suggested that the suppression of twinning is likely attributed to

Table 3
CRSSs of basal slip, prismatic slip, pyramidal slip and tension twinning of Mg at elevated temperatures [29].

Deformation system	Slip plane and slip direction	CRSS (MPa)
Basal $\langle a\rangle$	$\{0002\}\langle 11\bar{2}0\rangle$	0.6 MPa (473 K)
Prismatic $\langle a\rangle$	$\{10\bar{1}0\}\langle 11\bar{2}0\rangle$	3 MPa (573 K), 1 MPa (700 K)
Pyramidal $\langle a\rangle$	$\{10\bar{1}1\}\langle 11\bar{2}0\rangle$	3 MPa (573 K), 2 MPa (723 K)
Pyramidal $\langle c+a\rangle$	$\{10\bar{2}2\}\langle 11\bar{2}3\rangle$	4 MPa (573 K), 3 MPa (723 K)
Tension twinning	$\{10\bar{1}2\}\langle 10\bar{1}1\rangle$	2–3 MPa (independent of temperature)

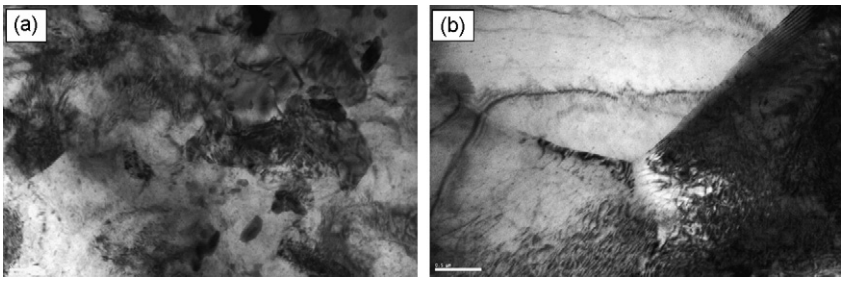

Fig. 9. TEM images of finial warm rolled TRC (a) and IC (b) samples.

the easy activation of non-basal slips, namely, decrease in CRSSs of non-basal slips.

It is known that the cross-slip tends to be more activated with increasing stacking fault energy (SFE) because the width of the extended dislocation is inversely proportional to the stacking fault energy. The activation of the prismatic ⟨*a*⟩ slip in Mg and its alloys corresponds to the cross-slip of screw dislocations from the basal plane to the prismatic plane [30]. Hirai et al. suggested that the stacking fault energy of Mg is decreased and DRX is induced by the addition of Al [31]. Also, Suzuki et al. [32] showed that the addition of Zn to Mg–Y alloy is effective for decreasing the stacking fault energy, resulting in the suppression of non-basal slips. Recently, Chino et al. [33] showed that it is possible to increase the stacking fault energy by elemental addition into α-Mg matrix, for example, by addition of Li and Ce. When the non-basal slips play an important role in deformation for Mg and its alloys, its rate-controlling process is the cross-slip of screw dislocations due to the Fridel–Escaig mechanism [34]. Therefore, it is likely suggested that the cross-slips are enhanced owing to an increase in the stacking fault energy caused by the high solid solubility of Mn in the present TRC alloy, resulting in the suppression of the twinning and the activation of the non-basal slip at the early and later stage during warm rolling. As for the influence of particles on the suppression of twinning, there were no systematical studies on particle/twin interaction in Mg, but it has been observed in Mg–1.6%Mn alloy that mechanical twinning is suppressed at particle spacing of ~300 nm, which is of the order of that revealed in Fig. 4b of ingot alloy [35]. However, contrary to Ref. [35], extensive twins were found in the present ingot alloy. Thus, it indicates that the suppression of the twinning at the early stage of rolling in TRC alloy is likely not attributed to the particle/twin interaction, but an increase in the stacking fault energy caused by the high solid solubility of Mn in α-Mg. Moreover, it is frequent to see that the twin formation tendency is a function of grain size in Mg alloys [36]. Coarse grains in Mg alloys will promote twin formation during deformation. The grain size in as-TRC sample is smaller than that in as-IC sample, which may be other reason not to commonly observe extensive twinning in as-TRC sample during warm rolling.

On the other hand, intermetallic phase particles can have a retardation effect on moving grain boundaries during grain growth. This so-called Zener-effect increases with increasing the number of particles and decreasing particle size. In the present study, the TRC sample shows more and finer primary dispersed particles than those of IC sample due to rapid solidification rate, as shown in Fig. 2. These particles can effectively pin the grain boundaries and retard the DRX, resulting in unrecrystallized microstructure during warm rolling. Upon annealing, static recrystallization takes place in the warm rolled TRC sample. High stored deformation energy and finer dispersed particles in warm rolled TRC sample will contribute to a high rate of nucleation and a low rate of grain growth caused by particle pinning, leading to the homogeneously fine-grained microstructure in the TRC sheet, as shown in Fig. 7a.

Tensile tests show that the TRC sample shows higher yield stress (YS) and ultimate tensile stress (UTS) as well as comparative elongation than those of IC sample, as seen in Table 2, indicating that the TRC sample exhibits superior mechanical properties compared to IC sample after warm rolling and subsequent annealing. The high strength of TRC sample is mainly due to the particle strengthening and solid solubility strengthening as well as fine-grain strengthening mechanisms resulting from the more and finer primary dispersed particles and smaller grain size, respectively. As for the reason why the post-annealed TRC sample showed slightly low elongation than that of the post-annealed IC sample regardless of finer grain size, authors consider that the small space between particles in TRC sample would easily induce the connection of holes initiated by dislocation interaction during the later stage of deformation, which may result in slightly low elongation compared to IC sample. The detailed mechanism will be further investigated.

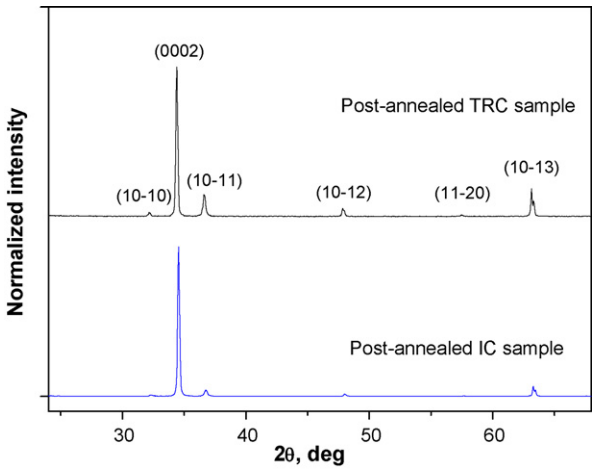

Fig. 10. X-ray diffraction patterns of post-annealed TRC and IC samples.

Moreover, it is well known that the distribution of (0 0 0 2) basal plane in magnesium alloys plays an important role on mechanical properties of Mg alloys at room temperature [3,29,37–39]. In the present study, simple XRD test was carried out on post-annealed TRC and IC samples, as shown in Fig. 10. XRD patterns of two samples exhibit the nearly same peaks, which likely means that post-annealed TRC and IC samples have similar texture characteristics. The highest (0 0 0 2) peaks demonstrate that post-annealed TRC and IC samples have similar (0 0 0 2) basal plane preferred orientation. For this reason, it is suggested that the influence of texture on mechanical properties of TRC and IC samples is likely similar between each other. So, the texture effect is ignored in this paper. The detailed study of texture on mechanical properties of TRC and IC samples will be further carried out.

5. Conclusions

(1) The microstructure of as-TRC AM31 + 0.2Ca alloy strip consisted of columnar dendrites in surface and equiaxed dendrites in center regions, and fine primary Al_8Mn_5 dispersed particles located on interdendritic boundaries as well as higher solid solubility of Al and Mn atoms in the α-Mg matrix due to the higher solidification rate than those of the conventional as-IC alloy.
(2) The warm rolled TRC samples exhibit intensively deformation band or shear band structures, as well as fine and homogeneously dispersed Al–Mn particles. No evident dynamic recrystallization (DRX) takes place during warm rolling process, which is more likely attributed to the effective Zener-effect by fine dispersed particles.
(3) The suppression of twinning at the early stage of rolling in TRC alloy sheet is likely not attributed to the particle/twin interaction, but an increase in stacking fault energy caused by the high solid solubility of Mn in α-Mg which results in the activation of non-basal slips, namely, decrease in CRSSs of non-basal slips.
(4) The TRC sample shows much higher yield stress and ultimate tensile stress and comparative elongation than those of IC sample. The high strength of TRC sheet is mainly due to the particle strengthening and fine-grain strengthening mechanisms resulting from the more and finer primary dispersed particles and smaller grain size, respectively. The present TRC alloy sheet has superior tensile properties compared to commercial IC one, suggesting the possibility of the development of wrought magnesium alloy sheets by twin roll strip casting.

Acknowledgements

The authors are grateful for the financial support of the Brain Pool Program of Korean Government performed by Korea Institute of Materials Science. This work was performed under the research project funded by the KIMS-NIMS international collaboration project. Authors thank Mr. S.S. Jung for assistance in preparation of specimen by twin roll casting and warm rolling.

References

[1] Y. Kojima, Mater. Trans. 42 (2001) 1154–1159.
[2] B.L. Mordike, T. Ebert, Mater. Sci. Eng. A 302 (2003) 37–45.
[3] L.W.F. Mackenzie, M. Pekguleryuz, Mater. Sci. Eng. A 480 (2008) 189–197.
[4] N. Stanford, M.R. Barnett, J. Alloys Compd. 466 (2008) 182–188.
[5] Y. Chino, M. Mabuchi, Scripta Mater. 60 (2009) 447–450.
[6] H.M. Chen, S.B. Kang, H.S. Yu, H.W. Kim, G.H. Min, Mater. Sci. Eng. A 492 (2008) 317–326.
[7] W.P. Peng, P.J. Li, P. Zeng, L.P. Lei, Mater. Sci. Eng. A 494 (2008) 173–178.
[8] H.M. Chen, S.B. Kang, H.S. Yu, J.Y. Cho, H.W. Kim, G.H. Min, J. Alloys Compd. 476 (2009) 324–328.
[9] W.J. Kim, B.H. Lee, J. Alloys Compd. 482 (2009) 106–109.
[10] S.S. Park, G.T. Bae, D.H. Kang, B.S. You, J. Nack, Kim, Scripta Mater. 61 (2009) 223–226.
[11] D.H. Kang, D.-W. Kim, S. Kim, G.T. Bae, K.H. Kim, J. Nack, Kim, Scripta Mater. 61 (2009) 768–771.
[12] Z.Y. Liu, S. Bai, S.B. Kang, Scripta Mater. 60 (2009) 403–406.
[13] Y.S. Park, S.B. Lee, N.J. Kim, Mater. Trans. 44 (2003) 2617–2621.
[14] Q.D. Wang, W.Z. Chen, X.Q. Zeng, et al., J. Mater. Sci. 36 (2001) 3035–3040.
[15] A. Suzuki, N.D. Saddock, J.W. Jones, et al., Scripta Mater. 51 (2004) 669–674.
[16] W.J. Kim, K.E. Lee, J.P. Park, et al., Mater. Sci. Eng. A 494 (2008) 391–396.
[17] S.S. Park, J.G. Lee, H.C. Lee, N.J. Kim, in: A.A. Lou (Ed.), Magnesium Technology, TMS, 2004, pp. 107–112.
[18] R. Kawalla, M. Oswald, C. Schmit, M. Ullmann, H.-P. Vogt, N.D. Cuong, METABK 47 (2008) 195–198.
[19] M. Ohno, R. Schmid-Fetzer, Z. Metallikd 96 (2005) 857.
[20] L.H. Han, H. Hu, D.O. Northwood, N.Y. Li, Mater. Sci. Eng. A 473 (2008) 16–27.
[21] T. Laser, M.R. Nurnberg, A. Janz, Ch. Hartig, D. Letzig, R. Schmid-Fetzer, R. Bormann, Acta Mater. 54 (2006) 3033–3041.
[22] L. Han, H. Hu, D.O. Northwood, N. Li, Mater. Sci. Eng. A 473 (2008) 16–27.
[23] M.R. Barnett, M.D. Nave, C.J. Bettles, Mater. Sci. Eng. A 386 (2004) 205.
[24] O. Sitdikov, R. Kaibyshev, T. Sakai, Mater. Sci. Forum. 419–422 (2003) 512.
[25] M.M. Avedesian, B. Baker (Eds.), ASM Specialty Handbook Magnesium and Magnesium Alloys, ASM International, Materials Park, 1999.
[26] T. Al-Samman, G. Gottstein, Mater. Sci. Eng. A 490 (2008) 411–420.
[27] Q.L. Jin, S.Y. Shim, S.G. Lim, Scripta Mater. 55 (2006) 843–846.
[28] L. Jiang, J.J. Jonas, A.A. Luo, A.K. Sachdev, S. Godet, Scripta Mater. 54 (2006) 771–775.
[29] Y. Chino, M. Mubuchi, Scripta Mater. 60 (2008) 447–450.
[30] J. Koike, T. Kobayashi, T. Mukai, H. Watanabe, M. Suzuki, K. Maruyama, K. Higashi, Acta Mater. 51 (2003) 2055–2065.
[31] K. Hirai, H. Somekawa, Y. Takigawa, K. Higashi, Scripta Mater. 56 (2007) 237–240.
[32] M. Suzuki, T. Kimura, J. Koike, K. Maruyama, Scripta Mater. 48 (2003) 997–1002.
[33] Y. Chino, M. Kado, M. Mabuchi, Mater. Sci. Eng. A 494 (2008) 3434–3449.
[34] A. Couret, D. Caillard, Acta Mater. 33 (1985) 1447–1454.
[35] N. Stanford, M. Barnett, Scripta Mater. 58 (2008) 179–182.
[36] M.R. Barnett, Z. Keshavarz, A.G. Beer, D. Atwell, Acta Mater. 52 (2004) 5013–5093.
[37] J. Bohlen, M. Nurnberg, J.W. Senn, D. Letzig, S.R. Angew, Acta Mater. 55 (2007) 2101–2112.
[38] R.K. Mishra, A.K. Gupta, P.R. Rao, A.K. Sachdev, A.M. Kumar, A.A. Luo, Scripta Mater. 59 (2008) 562–565.
[39] N. Stanford, D. Atwell, A. Beer, C. Daviesc, M.R. Barnett, Scripta Mater. 59 (2008) 772–775.